

Journal of Materials Chemistry A

Electrochemical Reactivity and Passivation of Organic Electrolytes at spinel MgCrMnO4 Cathode Interfaces for Rechargeable High Voltage Magnesium-Ion Battery

Manuscript ID Article Type: Paper Date Submitted by the Author: Complete List of Authors: Yang, Zhenzhen; Argonne National Laboratory; Joint Center for Energy Storage Research Cai, Jiyu; Argonne National Laboratory Wang, Evelyna; Argonne National Laboratory; Joint Center for Energy Storage Research Sultanov, Maksim; Argonne National Laboratory; Northern Illinois University Gao, Lihong; Joint Center for Energy Storage Research Wu, Xianyang; Argonne National Laboratory Liao, Chen; Argonne National Laboratory Liao, Chen; Argonne National Laboratory, Chemical Sciences and Engineering Division Wen, Jianguo; Argonne National Laboratory, Electron Microscopy Center Trahey, Lynn; Argonne National Lab Ingram, Brian; Argonne National Laboratory; Joint Center for Energy	Journal:	Journal of Materials Chemistry A
Date Submitted by the Authors: Complete List of Authors: Yang, Zhenzhen; Argonne National Laboratory; Joint Center for Energy Storage Research Cai, Jiyu; Argonne National Laboratory Wang, Evelyna; Argonne National Laboratory; Joint Center for Energy Storage Research Sultanov, Maksim; Argonne National Laboratory; Northern Illinois University Gao, Lihong; Joint Center for Energy Storage Research Wu, Xianyang; Argonne National Laboratory Liao, Chen; Argonne National Laboratory, Chemical Sciences and Engineering Division Wen, Jianguo; Argonne National Laboratory, Electron Microscopy Center Trahey, Lynn; Argonne National Lab Ingram, Brian; Argonne National Laboratory; Joint Center for Energy	Manuscript ID	TA-ART-05-2024-003765.R1
Complete List of Authors: Yang, Zhenzhen; Argonne National Laboratory; Joint Center for Energy Storage Research Cai, Jiyu; Argonne National Laboratory Wang, Evelyna; Argonne National Laboratory; Joint Center for Energy Storage Research Sultanov, Maksim; Argonne National Laboratory; Northern Illinois University Gao, Lihong; Joint Center for Energy Storage Research Wu, Xianyang; Argonne National Laboratory Liao, Chen; Argonne National Laboratory, Chemical Sciences and Engineering Division Wen, Jianguo; Argonne National Laboratory, Electron Microscopy Center Trahey, Lynn; Argonne National Lab Ingram, Brian; Argonne National Laboratory; Joint Center for Energy	Article Type:	Paper
Storage Research Cai, Jiyu; Argonne National Laboratory Wang, Evelyna; Argonne National Laboratory; Joint Center for Energy Storage Research Sultanov, Maksim; Argonne National Laboratory; Northern Illinois University Gao, Lihong; Joint Center for Energy Storage Research Wu, Xianyang; Argonne National Laboratory Liao, Chen; Argonne National Lab, CSE Chen, Zonghai; Argonne National Laboratory, Chemical Sciences and Engineering Division Wen, Jianguo; Argonne National Laboratory, Electron Microscopy Center Trahey, Lynn; Argonne National Lab Ingram, Brian; Argonne National Laboratory; Joint Center for Energy		08-Jul-2024
Storage Research	Complete List of Authors:	Storage Research Cai, Jiyu; Argonne National Laboratory Wang, Evelyna; Argonne National Laboratory; Joint Center for Energy Storage Research Sultanov, Maksim; Argonne National Laboratory; Northern Illinois University Gao, Lihong; Joint Center for Energy Storage Research Wu, Xianyang; Argonne National Laboratory Liao, Chen; Argonne National Lab, CSE Chen, Zonghai; Argonne National Laboratory, Chemical Sciences and Engineering Division Wen, Jianguo; Argonne National Laboratory, Electron Microscopy Center Trahey, Lynn; Argonne National Lab

SCHOLARONE™ Manuscripts

Electrochemical Reactivity and Passivation of Organic Electrolytes at spinel MgCrMnO₄ Cathode Interfaces for Rechargeable High Voltage Magnesium-Ion Battery

Zhenzhen Yang,^{a,b,*} Jiyu Cai,^a Evelyna Wang,^{a,b,} Maksim Sultanov,^{c,d} Lihong Gao,^b Xianyang Wu,^a Chen Liao,^{a,b} Zonghai Chen^a, Jianguo Wen,^c Lynn Trahey,^b Brian J. Ingram,^{a,b,*}

^a Chemical Sciences and Engineering Division, Argonne National Laboratory, Lemont, Illinois, 60439, USA

^b Joint Center for Energy Storage Research, Lemont, Illinois, 60439, USA

^c Center for Nanoscale Materials, Argonne National Laboratory, Lemont, Illinois, 60439, USA

^d Department of Physics, Northern Illinois University, Dekalb, Illinois, 60115, USA

Corresponding authors: yangzhzh@anl.gov, ingram@anl.gov, ingram@anl.

Abstract: Magnesium transition metal oxides such as MgCr_{2-x}Mn_xO₄ are the promising highvoltage and high-capacity cathode materials for rechargeable magnesium batteries (RMBs). Understanding and improving the chemical and electrochemical stability of the cathode-electrolyte interface (CEI) has been the primary technical emphasis to enable this category of cathode materials, which has been significantly underexplored. Herein, in this study we focus on investigating the fundamental mechanism of parasitic reactions at charged surface of high-voltage MgCrMnO₄ model cathode with different organic electrolytes. The aim is to reveal the underlying effect of anions and solvents responsible for the passivating behavior of cathode by using three exemplary anions: $[(CF_3SO_2)_2N]^-$ (TFSI-), Al $[OC(CF_3)_3]_4^-$ (TPFA-), and $[CB_{11}H_{12}]$ - (MC) and three solvents: diglyme (G2), triglyme (G3), and 3-methoxypropylamine (MPA). High precision leakage current measurements during potentiostatic hold reveal that the electrolyte solvent chemistry has a more profound impact than anion's on the passivation of the MgCrMnO₄ cathode surface during deintercalation of Mg²⁺. X-ray photoelectron spectroscopies exhibit the differences in CEI composition. Amine solvents like MPA show poor passivation due to higher degree of solvent decomposition, while a thin and anion derived CEI in glyme-based electrolyte is directly linked with the better passivating behavior on the cathode. Furthermore, we leverage the

knowledge from these findings to modify the electrolyte structure by adding a solvent additive, with the goal of reducing the parasitic reaction.

Keywords: High-voltage Mg spinel oxide, CEI formation, parasitic reactions, leakage current

1. Introduction

Novel battery compositions that transcend conventional lithium-ion configurations are needed to achieve paradigm-shifting progress in comprehensive electrified mobility and gridincorporated accumulation of renewable energy sources. Multivalent batteries including magnesium (Mg) and calcium (Ca), are enticing substitutes to lithium-ion batteries (LIBs) in terms of volumetric energy density and overall cell economics.^[1-3] After the original report of the Chevrel-phase cathode as applicable to magnesium-ion batteries, notable advancements have emerged in recent years in the development of novel, high-voltage transition metal oxide cathodes. A particularly promising chemistry is MgCr_{2-x} Mn_xO₄ with spinel structure for its high voltage (>3.0V vs. Mg²⁺/Mg) and high capacity (theoretically ~280mAh/g) for RMBs.^[4-7] There is an urgent demand for novel electrolytes with enhanced electro-anodic and chemical stability to enable a reversible high voltage cathode chemistry. [1, 8-9] Furthermore, electrolyte design must consider Mg²⁺ ion conduction, optimal efficacy in the processes of Mg plating and stripping, as well as its compatibility on the Mg metal anode to realize the high-energy full-cell configurations. Due to their limited oxidative stability and high reactivity toward cathodes and other cell components, early-stage developed electrolytes based on organometallic compounds assisted by chloride ions dissolved within ethereal solvents, are encountering challenges in their practical functionality. [10-11]

Several electrolyte design strategies have been reported in the literature. Due to the significant polarization of Mg^{2+} , the concept of employing bulky monocharge anions was introduced, aiming to weaken the interaction with Mg^{2+} in the electrolyte through delocalized electrons. Therefore, the exploration of Mg salt with weakly coordinating anions (WCAs) eliminating the need for chlorine components has governed interest towards more pragmatic Mg electrolytes, and offer a basis for evaluating high-voltage cathode materials. Initial attempts using $Mg(BH_4)_2$ showed limited anodic stability around $\approx 2V$ vs. Mg. Other categories of WCAs

featuring B-centers (or Al-centers) have displayed promising electrochemical activities with widened electrochemical windows of up to 3.8 V vs. Mg as suitable supporting electrolyte anions for Mg^{2+} . Examples of these WCAs include $B[O_2C_2(CF_3)_4]_2^{-,[18]}$ ($CB_{11}H_{12}$)-closo- $Al[OCH(CF_3)_2]_4]^{-,[21]}, Al[O_2C_2(CF_3)_4]_2^{-,[22]}$ B(Otfe)₄]-,^[20] monocarborane,[19] $Al[OC(CF_3)_3]_4^{-.[23]}$ The $Al[OC(CF_3)_3]_4^{-}$ (abbreviated as TPFA) anion is of particular interest because of its reported wide electrochemical windows for both cathodic and anodic electrochemical stability. [23] In addition to selecting appropriate anions, the choice of solvent has decisive role in ensuring compatibility between the cathode and electrolyte. Solvents that have been empirically confirmed to facilitate reversible Mg plating and stripping are limited to ethers. Searching for more suitable solvents for Mg batteries poses a significant challenge, as multiple issues such as Mg²⁺ ion transport, efficient Mg²⁺ coordination, desolvation energies at the interface, and impurity, must be addressed simultaneously. Recent discoveries involving cosolvents like methoxyethyl-amines and hydrofluoroethers with tailored coordination to Mg²⁺ offer valuable insights and may provide a framework for exploring alternative solvents in future research efforts.[12-13, 24-25]

Recent studies suggest that in Mg batteries, the rate of interfacial charge transfer may be a limiting factor, potentially more significant than solid bulk diffusion.^[8, 26] While the challenges related to the interfacial behavior of the Mg anode are well-recognized and investigated, the interfaces on the high-voltage cathode, which involve more complex processes, remain largely unexplored and still an emerging area of research.^[10, 27-28] Cathodically stable electrolytes are typically evaluated for their oxidative stability through basic voltammetry measurements on Pt/Al/SS substrates, rather than on realistic cathode surfaces. Particularly, due to limited Mg²⁺ transport and Mg penetration depth, reducing particle size in cathode materials proves to be a viable approach to enhance electrochemical performance, but it leads to increased surface area and (electro-)chemical reactivity. Since these side reactions on the cathode surface is expected to influence the measured cyclability and capacity, it is essential to conduct a thorough evaluation of these electrolyte materials and any possible interphases they may form when exposed to actual transition-metal oxide cathode surfaces.

In the context of addressing this knowledge gap, this work aims to investigate how the structures of anions and solvents influence their stability and the extent of oxidative decomposition

during the cathode charging process. We utilize a systematic approach, as illustrated in Figure 1, from an electrolyte matrix comprised of three anions: ([(CF₃SO₂)₂N]⁻, TFSI), Al[OC(CF₃)₃]₄⁻ (TPFA), and [CB₁₁H₁₂] (MC) and three solvents: diglyme (G2), triglyme (G3), and 3methoxypropylamine (MPA). The impact of anion species is investigated in a fixed G3 solvent and the role of solvent is compared by using a constant Mg[TPFA]₂ solution. The rationale for selecting these specific anions and solvents arrays was to evaluate a diverse chemical functionality with high redox stabilities for the high-voltage cathode material. This study systematically compares electrolyte coordination structure by FTIR, quantifies parasitic reactions by in situ monitoring leakage current, and assesses the impact of the passivation surface layer formation through XPS analysis. This methodology will identify the origins of instability and chemicalstructural characteristics that exhibit correlations with desired electrochemical properties against representative high-voltage cathode MgCrMnO₄. Our primary objective is to identify suitable components for an efficient cathode-electrolyte interface (CEI) to reduce the parasitic reactions, prioritizing a focus on understanding rather than emphasizing engineering optimizations tailored to a specific chemistry. Lastly, we intend to provide design guidelines for future development of a well-functioning CEI, achieved through either modifying the electrolyte formulation using additives to cathode materials.

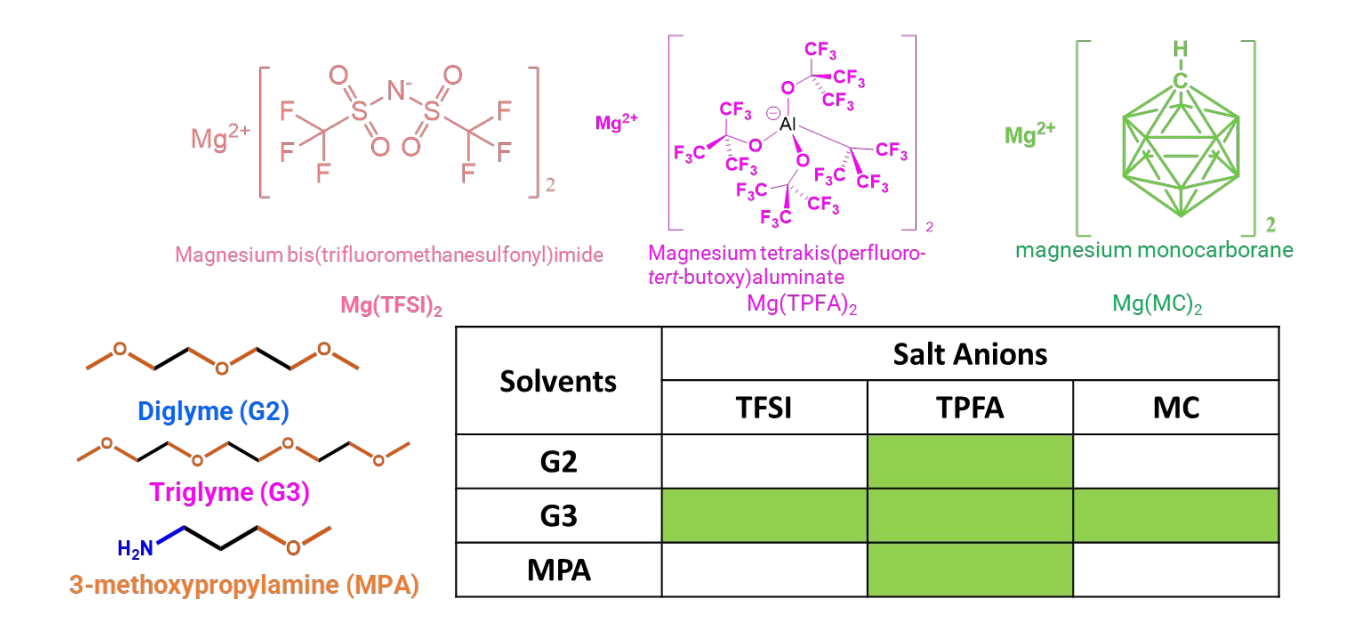


Figure 1. The electrolyte matrix includes a variety of solvents: diglyme(G2), triglyme(G3) and MPA; and salt anions: $[(CF_3SO_2)_2N]^-$ (TFSI-), Al $[OC(CF_3)_3]_4^-$ (TPFA-), and $[CB_{11}H_{12}]^-$ (MC). The concentration for all the solutions is 0.1M.

2. Results and Discussion

2.1 Electrolyte structure

The solvation structure of electrolytes is critical to its stability and reactivity on Mg electrode surface. [29] To investigate the interplay between anions and solvents, we conducted IR analysis on various electrolyte compositions based on the matrix in Figure 1. The effect of anion dissolved in G3 is shown in Figure 2a, where a distinct IR band is observed between 1000~1100 cm⁻¹ for all the solutions. This is attributed to the vibrations of the solvent G3 conformers, including C-O-C, C-C, and C-O stretching modes within the bulk. [30] The peak at 1101 cm⁻¹, evident in the pure G3 (black line), decreases slightly in intensity with the addition of Mg²⁺. Simultaneously, new peaks emerge at wavenumbers of 1059 cm⁻¹ and 1134 cm⁻¹, corresponding to the G3 molecules coordinated to Mg²⁺ ions to form the solvent separated ion pairs (SSIPs) like [Mg(G3)₂]²⁺ complex.^[31] Adding Mg[TFSI]₂ in G3 results in a small characteristic peak at 740 cm⁻¹, attributed to the CF₃ bending vibration coupled with the S-N-S stretching vibration of the free TFSI component. In comparison with the IR spectrum of pure Mg[TFSI]₂ crystal, the absence of blue-shift of this vibration peak in the TFSI/G3 spectrum implies that Mg²⁺ preferably to form. The addition of Mg[TPFA]₂ in G3, on the other hand, reveals the existence of four strong characteristic vibrational bands ranging from 1200 to 1300 cm⁻¹ and two singular bands at 975 cm⁻¹ and 724 cm⁻¹. These were attributed to the mixed C-C, CF₃ symmetric and asymmetric stretching modes (~1277 cm⁻¹, 975 cm⁻¹), and Al-O-C vibration mode (~ 1221 cm⁻¹) within the [TPFA]⁻ anion.^[23] In comparison to the crystalline Mg[TPFA]₂, the blueshift of the bands, for example at 1221 cm⁻¹ and 975 cm⁻¹, suggests a structural change in the anion due to the coordination of TPFA- to Mg²⁺ with G3. This finding is consistent with the detection of [Mg(TPFA)G3]⁺ contact ion pairs (CIPs) formation by NMR in previous work. [23] A similar trend was observed for the MC/G3 system. Solvated with G3 leads to the formation of contact ion pairs in the solution, characterized by the blueshift of IR bands at 716 cm⁻¹ representing the Al-O-C vibration mode and CF₃ stretching modes, when compared to reference of the pure Mg[MC]₂ salt. Additional new small peaks, corresponding to the vibration modes of C-CF₃ groups and the

deformation mode of the -CF₃ groups, were detected at 975 and 1221 cm⁻¹, respectively, indicating the bound MC to G3 in the solution.

The impact of the three solvents with 0.1M Mg[TPFA]₂ on the electrolyte structure is readily apparent in Figure 2b. All TPFA⁻ signals exhibit a blueshift relative to the crystalline Mg[TPFA]₂, attributed to TPFA⁻ in a Mg-TPFA contact ion pair. In G2, a highly similar pattern to G3 was observed, implying the formation of analogous ion pairs in both solvents. However, the IR signals of the MPA system are different from glyme-based solvents. For example, the peaks at 852 cm⁻¹, 1024 cm⁻¹, and 1455 cm⁻¹, corresponding to symCF₃ modes of TPFA⁻ in the Mg-TPFA ion pair diminishes when dissolved in MPA. In contrast, the peaks centered at 968 cm⁻¹ and 1221cm⁻¹ intensifies from G2 to MPA. The presence of the N-H bond in MPA may influence the dissociation of Mg[TPFA]₂ in this solvent. MD simulations has demonstrated 95.1% dissociation in TFSI/MPA electrolyte.^[32]

The formation of ion pairs in each electrolyte is indeed a delicate balance between cation solvent and anion-cation interactions, potentially arising from electrostatic, hydrophobic, or charge transfer interactions. [33] Thus, the pairing process may be triggered by the unique ionspecific character of each solvent or anion. Figure 1c illustrates the possible SSIPs and CIPs formed with the selected anions and solvents. In the SSIPs, the cation's first solvation shell is composed of multiple solvent molecules. For example, in fully solvated SSIP, Mg²⁺ is surrounded in a ring by two G2/or G3 molecules and forms a six-coordinated bridge with the oxygen atom in the glymes. [33] MPA shows even stronger coordination with Mg by the strengthened Mg–N bonds to form fully coordinated [Mg(MPA)₃]²⁺.[12] While in the CIPs, this shell includes a mix of one or more anionic species and several solvent molecules to form fully coordinated or undercoordinated structures. [29] The relative abundance of SSIPs and CIPs in the bulk electrolyte is determined by the strengths of Mg²⁺-solvent and Mg²⁺-anion dynamic interactions. We selected WCAs for this study, so that SSIPs are the predominant ionic species in these electrolytes. However, a small amount of CIPs cannot be excluded, as supported by the FITR data in Figure 2a-b and our previous work. [23, 34] Compared to bulky TPFA and MC anions that have the steric hindrance, more electron localized TFSI⁻ anion tends to be form relatively stronger CIPs.^[15] The different electrolyte solvation environment significantly affects its electrochemical properties, including transport and desolvation process at both anode and cathode electrode interface.

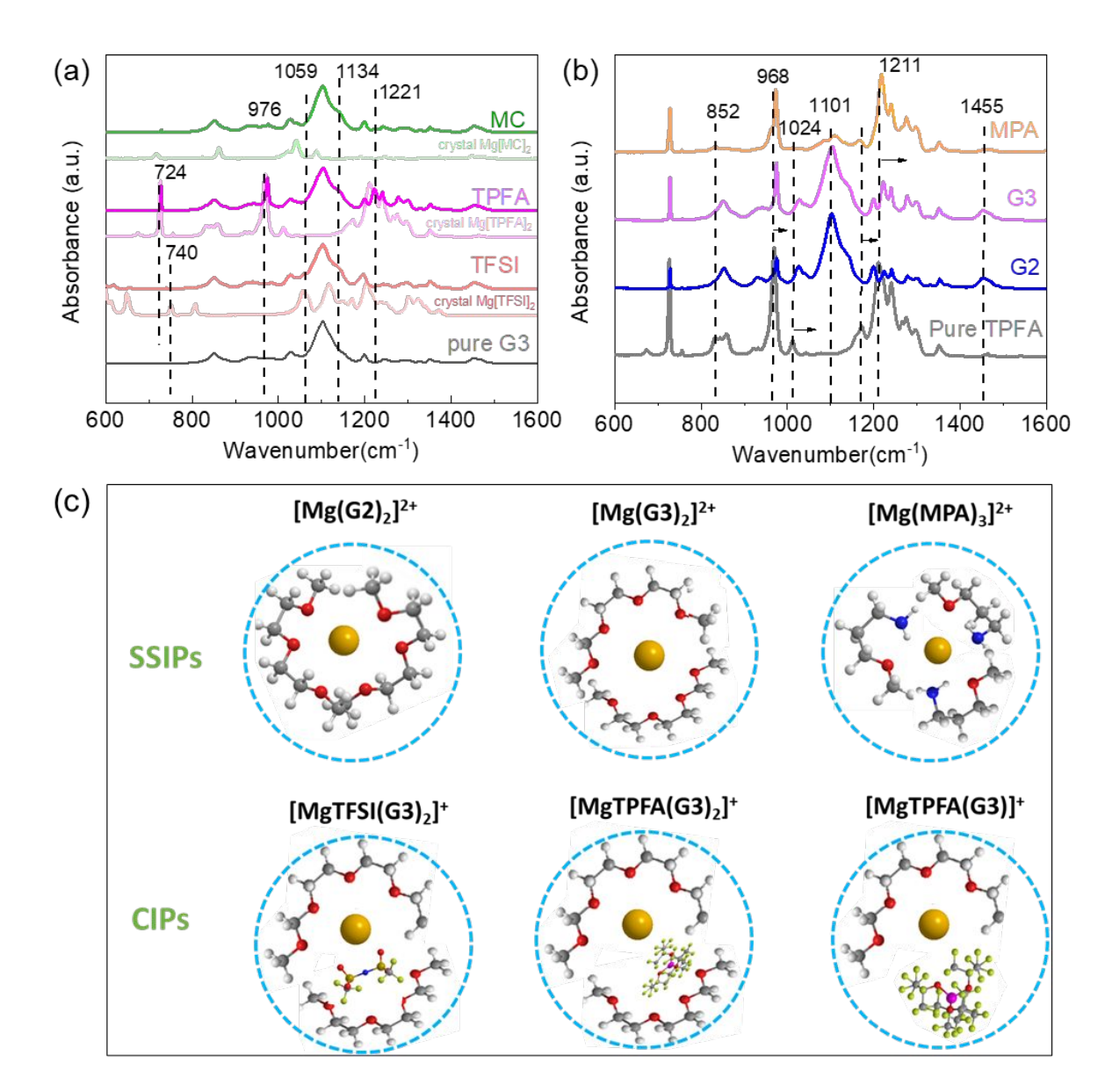


Figure 2. The FTIR spectra within the spectral regions of 600-1600 cm⁻¹ for different solutions: (a) Mg[TFSI]₂, Mg[MC]₂ dissolved in G3; (b) 0.1M of Mg[TPFA]₂ in G2, G3, and MPA. The pure salts of Mg[TFSI]₂, Mg[TPFA]₂, Mg[MC]₂ and pure G3 solvent were also examined and used references. (c) Schematics of the Mg-ion solvation structure illustrating the possible SSIPs and CIPs in the electrolytes.

2.2 Electrochemical performance

Reductive behaviors of the prepared electrolytes during Mg plating/stripping tests were first evaluated using cyclic voltammetry (CV) on a Pt working electrode. For most Mg electrolytes, we have found that a preconditioning step is necessary to remove reaction impurities and achieve

optimal Mg deposition/stripping efficiency, though initial purified materials used. [35-36] Figure 3ab shows CV data on a Pt electrode cycled in 0.1 M electrolytes after conditioning process with the protocol proposed in our previous study. [35] The TFSI/G3 results in a much lower current density and is obscured by other two data sets. Individual CVs and summarized electrochemical performance values including CE, plating/stripping potentials are available in Figure S1 and Table S1. The highest apparent Coulombic efficiency (CE) in Mg plating/stripping processes was realized in the TPFA/G3-based electrolyte (~87%), whereas the lowest efficiency was observed in the TFSI/G3 electrolyte (~23%). Furthermore, TPFA/MPA electrolyte exhibited higher current density, signifying a higher level of Mg²⁺ ions available for redox reaction. This is due to faster Mg mobility towards the electrode and a more compatible or reactive interface which lead to more efficient charge transfer, when a fully coordinated SSIP [Mg(MPA)₃]²⁺ are effective charge carriers.[12, 34] A parallel trend of distinctions was evident when comparing the onset Mg plating/stripping potentials. TPFA and MC-based electrolytes exhibited overpotentials of 250 and 420 mV, respectively, while TFSI-based electrolytes displayed notably larger overpotentials for Mg stripping, reaching up to 2320 mV. It is believed that the overpotentials observed in the stripping curves are closely linked to the Mg surface passivation from different parasitic electrolyte reduction mechanisms such as the reaction with the trace impurities in the electrolyte. [36]

The oxidative stability of these electrolytes was investigated through traditional linear sweep voltammetry with a scan rate of 1 mV/s on Pt electrodes, and the results are compared between two groups in Figure 3c and d. For a more direct evaluation of oxidative stability, we define the oxidative potential limit as the voltage at which the anodic current reaches 0.01 mA/cm², slightly exceeding the background current of all electrolytes in LSV measurements. Then the oxidative potential limits listed in Figures 3c-d show that they increase in the order of TFSI < TPFA < MC for anion group, and MPA < G2 < G3 for solvent group, respectively. The remarkable stability of the MC anion is attributed to its highly delocalized chemical bonding and a substantial HOMO–LUMO gap.^[37] With MPA, an early peak emerges within the voltage range of 3.5–4.0 V, stabilizing up to 4.12 V, followed by an exponential increase in current density. This indicates that, although MPA has demonstrated excellent reductive performance for Mg plating/stripping in both this study and previous reports,^[12, 34] it has lower anodic stability compared to the other two glyme solvents. This is due to the presence of a nucleophilic nitrogen atom with a lone pair of electrons in this primary amine, making it susceptible to electro-oxidation.^[38]

Analyzing the reductive and oxidative performance onto Pt electrode offers valuable insights into the characteristics of electrolyte stability. It is more important to evaluate its ability to support reversible Mg insertion/extraction in a real-world cathode. Next, we examined the coin cell performance of the previously reported ~3V cathode composed of MgCrMnO₄ to demonstrate the redox chemistry with each electrolyte, given its high theoretical specific capacity and the solvent-free storage characteristics of Mg²⁺ in electrolytes.^[5, 39] Figure 3e and f displayed the initial cycling performance versus carbon cloth in half-cells cycled between potential range of -1.2 V and 1.2 V (corresponding to a range of 3.2–0.8 V relative to the Mg/Mg²⁺ using the calibration data from ref [5]). Among all the cells, the TPFA/G3 cell exhibits the highest charging capacity approximately 46 mAh/g and subsequent discharging capacity of 35 mAh/g, accompanied by the relatively smallest redox potential hysteresis. While the TFSI/G3 and TPFA/MPA cells provide much lower capacities and larger overpotentials above 2V. The results further confirm the solventanion interactions in the electrolyte play a significant role on the cell performance. However, the overall observed large polarization and small capacity can be attributed to a range of complex issues, encompassing sluggish Mg²⁺ kinetics in the bulk, poor desolvation of Mg²⁺ and unfavorable interfacial charge transfer processes at the interfaces, and the formation of passivation layers on the cathode. The former challenge associated with sluggish Mg²⁺ mobility within the lattice can be significantly ameliorated by cycling the cells at elevated temperatures (e.g., 95 °C or 110°C), as demonstrated in previous studies which showed a notable increase in the capacity and reduction in the extent of polarization.^[4-5] Other interfacial-related issues will be further examined by investigating the interfacial reactions occurring on the cathode surface in the following sections.

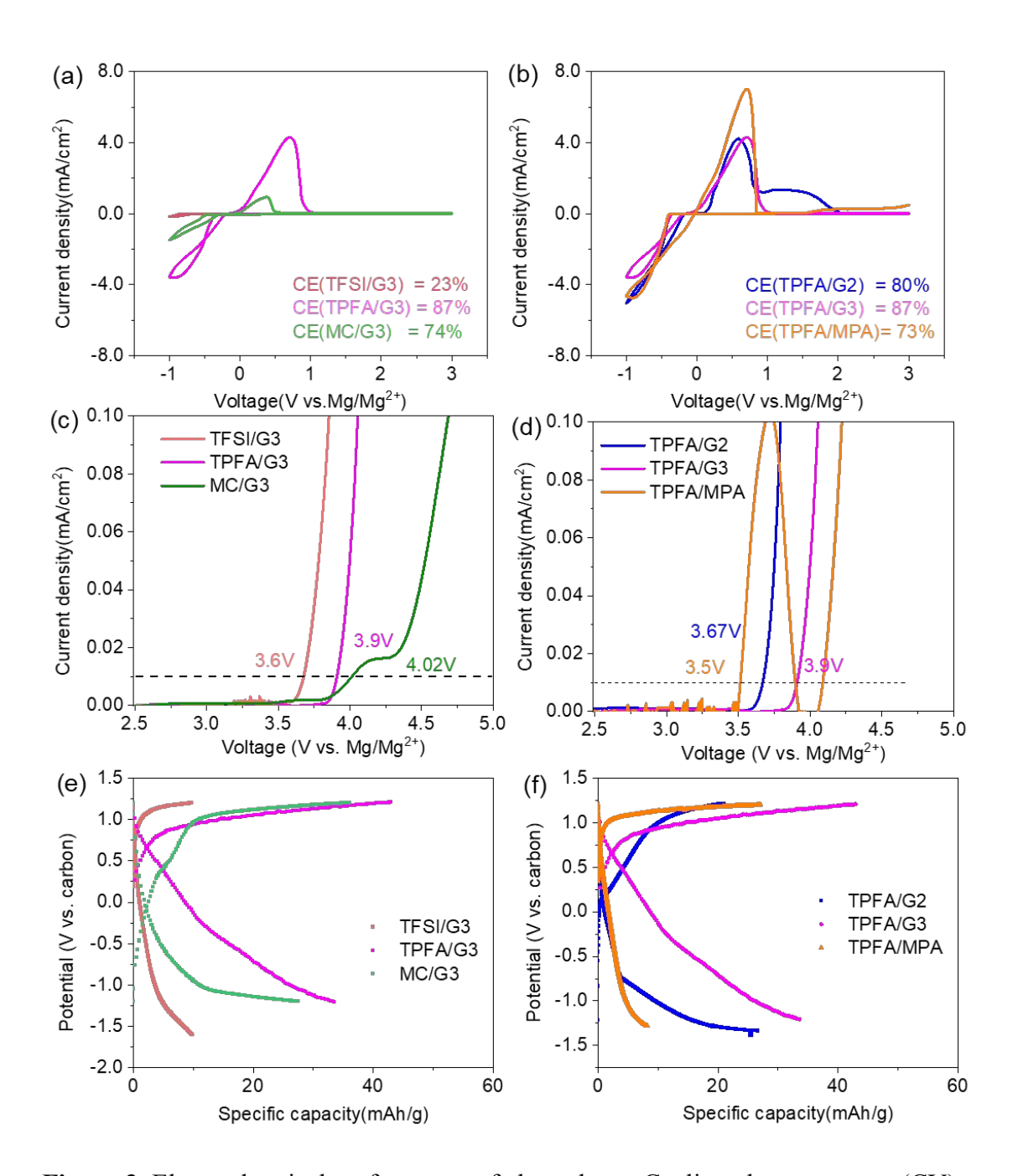


Figure 3. Electrochemical performance of electrolytes. Cyclic voltammograms (CV) comparison for (a) different anions in G3 of 0.1 M electrolytes; and (b) different solvents with TPFA⁻ anion; Linear sweep voltammograms (LSV) comparison for (c) different anions in G3 of 0.1 M electrolytes; (d) different solvents with TPFA⁻ anion. In these experiments, three-electrode cells were used in which a platinum electrode served as the working electrode, magnesium as the counter electrode/reference electrode. The scan rate for CV is 25mV/s and for LSV is 1mV/s. First galvanostatic charge-discharge curves comparison for (e) different anions in G3 of 0.1 M

electrolytes; (f) different solvents with TPFA⁻ anion. Coin cells cycled at 25 °C with MgCrMnO₄ cathode paired with a carbon counter electrode.

2.3 Electrolyte parasitic reactions on charged MgCrMnO₄ cathode

The susceptibility of electrolyte to oxidation and resulting cathode electrolyte interphase (CEI) is more dependent on the charging process. Therefore, an assessment of electro-oxidative stability and side reactions during charging was conducted on MgCrMnO₄ cathode in half-cells using our in-house, high-precision leakage current (HpLC) measurement system. We quantitatively assess the rate of parasitic reactions occurring solely on high surface area cathode in featuring controlled potentials by measuring the real-time static leakage current, but without considering the contribution and complexity arising from the chemical interaction between Mg metal and the electrolyte. Figure 4a shows the average measured leakage current as a function of time during potentiostatic hold from 0.6 V to 1.2 V vs. carbon cloth (or 2.65 V to 3.25 V vs. Mg/Mg²⁺) in sequence for cell with TFSI/G3 electrolyte. Data for other electrolytes can be found in Figure S2. In all cells, within the initial hours, there is a pronounced decline in current from the initially galvanostatic charging current. This initial drop signifies the relaxation of concentration gradients within the cell. The relaxation time of the system depends on characteristic lengths and diffusion coefficients for the electrolyte, electrode, and active material, as per Doyle et al[40] and Vadivel et al. [41] The relaxation time, as depicted in Figure 4a, is approximately 5 hours. Following cell relaxation, the leakage current stabilizes at a constant, albeit non-zero level. This constant current characterizes the rate of ongoing parasitic reactions, which continually supply electrons from the electrolyte to the cathode interface. Its value can be determined by fitting the decaying current profile using an exponential decay function $(y = A*exp(-x/t) + y_0)$, [42] shown in Figure 4b. Figure 4c and d compare this static current (y₀, normalized to the active mass of MgCrMnO₄) as a function of potentials and electrolyte components. As the potential hold voltage rises, the static current increases in the cells with the order of TFSI > MC \ge TPFA in the anion group, and MPA > G3 > G2 in the solvent group. The trend in the anion group is consistent with the previous reports that electron-withdrawing functional group (such as -CF₃), or HCB₁₁H₁₁⁻ cage, increase the anodic stability for the salts.^[43] While for the solvents, MPA shows the highest leakage current, signifying its lack of electro-oxidative stability for high-voltage Mg cathodes, despite displaying favorable reductive performance on Mg anodes in Figure 3b and previous work.^[34] Comparing the two

groups indicates the solvent has more influence on the leakage current than the anion. It is also noteworthy that this increasing trend varies across different electrolytes. For instance, the steady leakage current exhibits an approximate exponential increase in relation to the working potential for the cells containing TFSI/G3, TPFA/G3, and TPFA/G2. This indicates at a low potential < 0.9 V, the parasitic reactions are slow and probably dominated by the chemical reaction between the cathode and active electrolyte species at the interface. [44] Concurrently, at elevated potentials above 0.9V (~2.95V vs. Mg/Mg²⁺), the steady leakage current becomes more significant primarily stemming from the direct electrochemical oxidation of electrolyte component at de-magnesiated cathode surface. We hypothesize that when more Mg extracted from MgCrMnO₄ with higher potentials upon charging, it induces more Mg vacancies and surface-active oxygen (i.e. accumulation of O²-). This phenomenon may change the surface adsorption behaviors (e.g. strengthen the bonding between glyme solvent and Mn atoms), thereby promoting electron transfer from solvent molecule and subsequent decomposition. A recent theoretical study by DFT calculations confirmed a direct correlation between the DME(dimethoxyethane) decomposition and the demagnesiation reaction of the spinel oxides.^[45] A demagnesiated surface promotes the dissociated adsorption of DME fragments, facilitating smooth charge transfer. While the other two electrolytes (MC/G3 and TPFA/MPA) show a more gradual and linear increase in the current with the holding potentials, implying these two electrolytes have limited stability on cathode. Of the chemical bonds listed in three studied solvents, the N-C bond is identified as the weakest. The amino group in MPA can be relatively easily liberated, and the resulting hydroxyl group is susceptible to oxidation. On the other hand, these threshold potential values measured by HpLC on real cathode are notably lower than those determined through above LSV measurements on Pt, converting to the voltage versus Mg/Mg²⁺ (top x-axis in Figure 4c and d). The trend in relative stabilization, particularly the influence of the solvent between G2 and G3, is reversed when comparing the results in Figure 3d and 4d. This comparison emphasizes the electrolyte reactivity challenges imposed at realistic high voltage cathode surfaces.

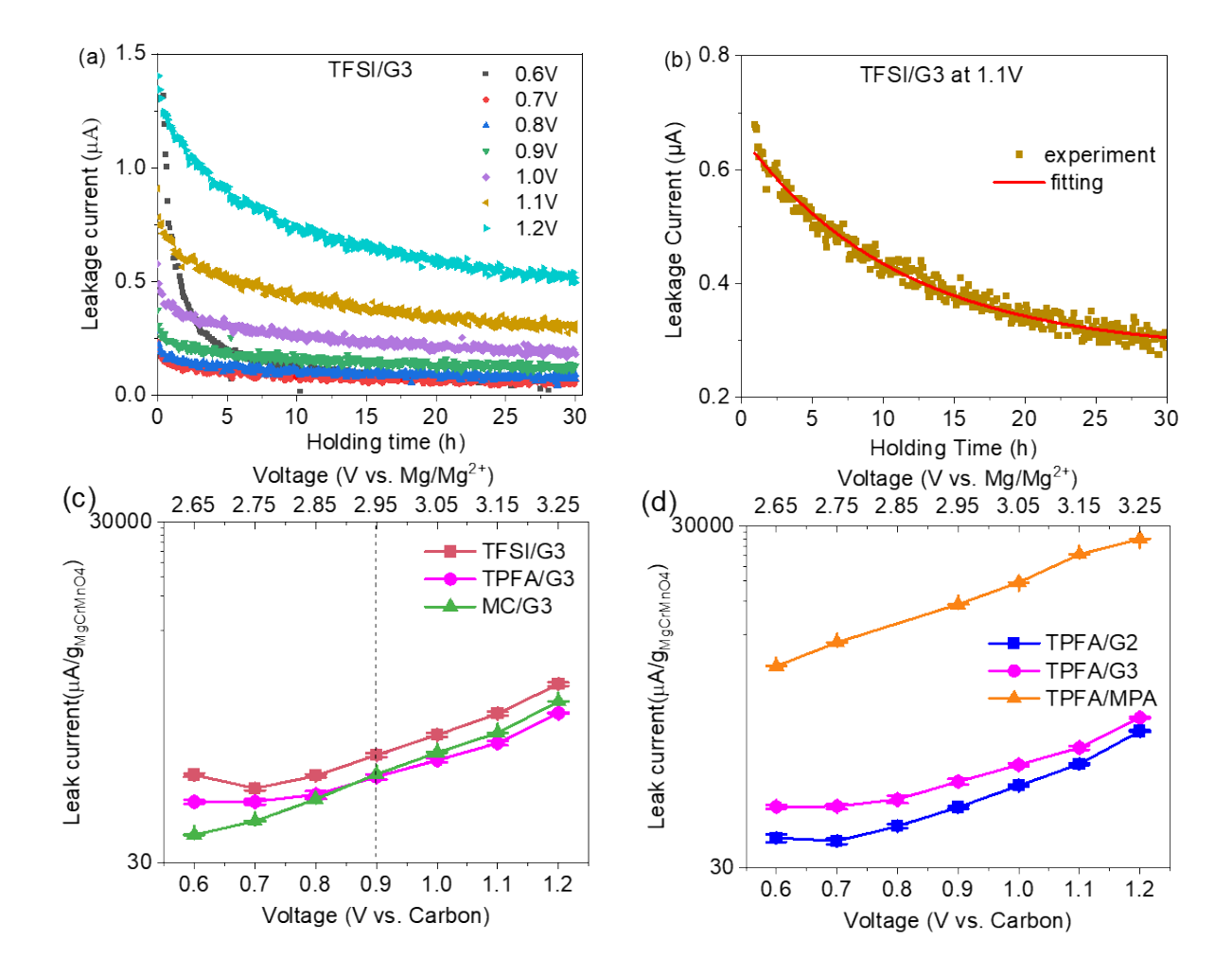


Figure 4. (a) Dependence of the steady state leakage current on the working potential in half cells verse carbon cloth for TFSI/G3 electrolyte as an example; (b) Typical raw data collected by fitting to extract the steady state leakage current by holding the voltage of the cell at 1.1 V for 30 hours; (c) Comparison of the steady state leakage current, normalized by the active mass of MgCrMnO₄, between three anions; (d) Comparison of the steady state leakage current between three solvents. The fittings are all 95% confidence intervals.

2.4 CEI formation upon charging

The disparity in the above parasitic reactions is related to build-on film formation and chemical variations in the CEI. X-ray Photoelectron Spectroscopy (XPS) was then conducted after HpLC testing to delve deeper into this matter. The CEI components observed on the charged cathode surface include relatively high concentrations of C, O, F, N, and Mg, along with small amounts of sulfur (S)/or Boron (B)/or Aluminum (Al) from each anion decomposition. The atomic

percentage of CEI components quantified from XPS measurement are shown in pie chart of Figure 5a. Corresponding high-resolution spectra and deconvolution of peaks for the major components C, O and F are provided in Figure 5b and c, for the anion and solvent group, respectively. Overall, the CEI components exhibited a clear dependence on the electrolyte composition, suggesting that the CEI can be tuned by modifying the electrolyte composition. Meanwhile the CEI thickness should be thinner than the probing depth of \sim 10 nm (XPS penetration depth), as the lattice oxygen around 529 eV and presence of Cr/Mn is clearly visible for all samples. Based on a higher Cr and Mn signal from the underlying cathode, both MC and TPFA cells exhibit a thinner CEI among all cells. This trend is corroborated by additional TEM/EDS observations, which indicate the average surface layer thickness for TPFA/G3 and MC/G3 is approximately 5 ± 0.8 nm, as shown in Figure 5d. The TFSI cell exhibited a thicker surface layer consisting of N, S, F and an average thickness of 10 nm. The CEI layer in the MC and TPFA cells provided more uniform and dense coverage than the one formed with TFSI. However, due to the much limited nanoscale information from TEM, we use XPS results in the following sections to assess the dependency of the CEI on electrochemical performance and other factors.

Comparing the anions group, MC and TPFA lead to decreased total carbon atomic ratio with fewer organic species including -C-OR, -C=OR and-C=O-OR, implying reduced interfacial side reactions from solvent decomposition. Meanwhile, the fluorine content increases in the CEI due to the CF₃- group in TPFA structure, distinguishing it from TFSI. It's noteworthy that the atomic ratio of Boron is significantly lower than that of Al and N/S. It is probable that the Boron species may be buried under the organic constituents of the CEI, or alternatively, that the electrooxidation of MC electrolyte produces more soluble fragments containing Boron. The first assumption is substantiated by XPS depth profiling, which reveals twice the amount of B within the inner CEI (Figure S3a). A higher distribution of Al in the inner layer of CEI is also observable for the TPFA cells (Figure S3b). In this scenario, the larger content of inorganic compounds (e.g. AlF₃, MgF₂, Figure 5b, Figure S3c) proximal to the charged cathode surface from the decomposed salt serves as a stabilizing agent for the electrode, thereby preventing the continued degradation resulting from solvent compounds. There might exist thermodynamically and kinetically favorable pathways for consuming anions in these two electrolytes, affecting the rate of electron transfer and the extent of anion decomposition. As discussed in section 2.1, much weaker CIPs form in TPFA/G3 and MC/G3, potentially facilitating desolvation processes and subsequent decomposition at the charged interface and leading to anion-rich CEI. Another possibility of anion-derived CEI products is the distinct decomposition pathways and cleavage mechanisms for various bare anions during the oxidation process with presence of transition metals like Mn considering its strong catalytic effect. It has been demonstrated that free anions exhibit higher susceptibility to oxidation compared to contact ions at the cathode surface. [46] Thus, free TPFA- undergo decomposition more easily and potential pathway includes the cleavage of a C-O, Al-O, and C-F bond and contribute to the formation of MgAl₂O₄/Al_xF_v-rich CEI (Figure 5b). The different distribution of CEI between TPFA and MC also confirms the previous mechanistic studies by calculation which predict a significant difference in the factors controlling the kinetics of Al/B-O bond breaking, C-O bond breaking, and C-F bonding breaking decompositions between alkoxy-borate [B(OR)₃] and alkoxy-aluminate [Al(OR)₃] salts. [46] TFSI anions decompose, forming CEI components such as SO_xF, –SO₂–, –S(O)–, and CF₃ through C-S, N-S, and C-F bond cleavages. (F1s and S2p spectrum in Figure 5b). Figure 5e summarizes a schematic diagram outlining the primary degradation pathways proposed for these electrolytes in this study. Identifying a detailed origin of CEI requires more completed experiments and theoretical calculations, which are beyond the scope of this work and will be addressed in a future study.

Within the solvent comparison group, it is evident that there is a substantial increase in C content and a significant decrease in F content when transitioning from G2 to MPA. The discrepancy in spectra, indicative of possible C-, O- and F-species, appears more pronounced within the solvent group compared to the anion group. Again, the strength of coordination between the solvent and the cathode surface plays a pivotal role in determining the extent of electrolyte decomposition. Additionally, there is a notable increase in N content for MPA, signifying a greater oxidation instability and incorporation of solvent decomposition species in the formation of the CEI. When we correlate these observed patterns with the electrochemical performance in section 2.2 and leakage currents discussed in section 2.3, it becomes apparent that the primary components of the CEI, specifically C, and F, can be directly associated with the leakage current. A higher leakage current is noted in CEI compositions with organic-rich content. Conversely, a thin CEI with higher F chemical environments from electron-withdrawing ligands like in TPFA can reduce leakage current, enhance cathode passivation and performance. Therefore, in the next section, we seek to provide guidance for electrolyte design to utilize this beneficial effect of F chemistry to stabilize Mg cathode surface.

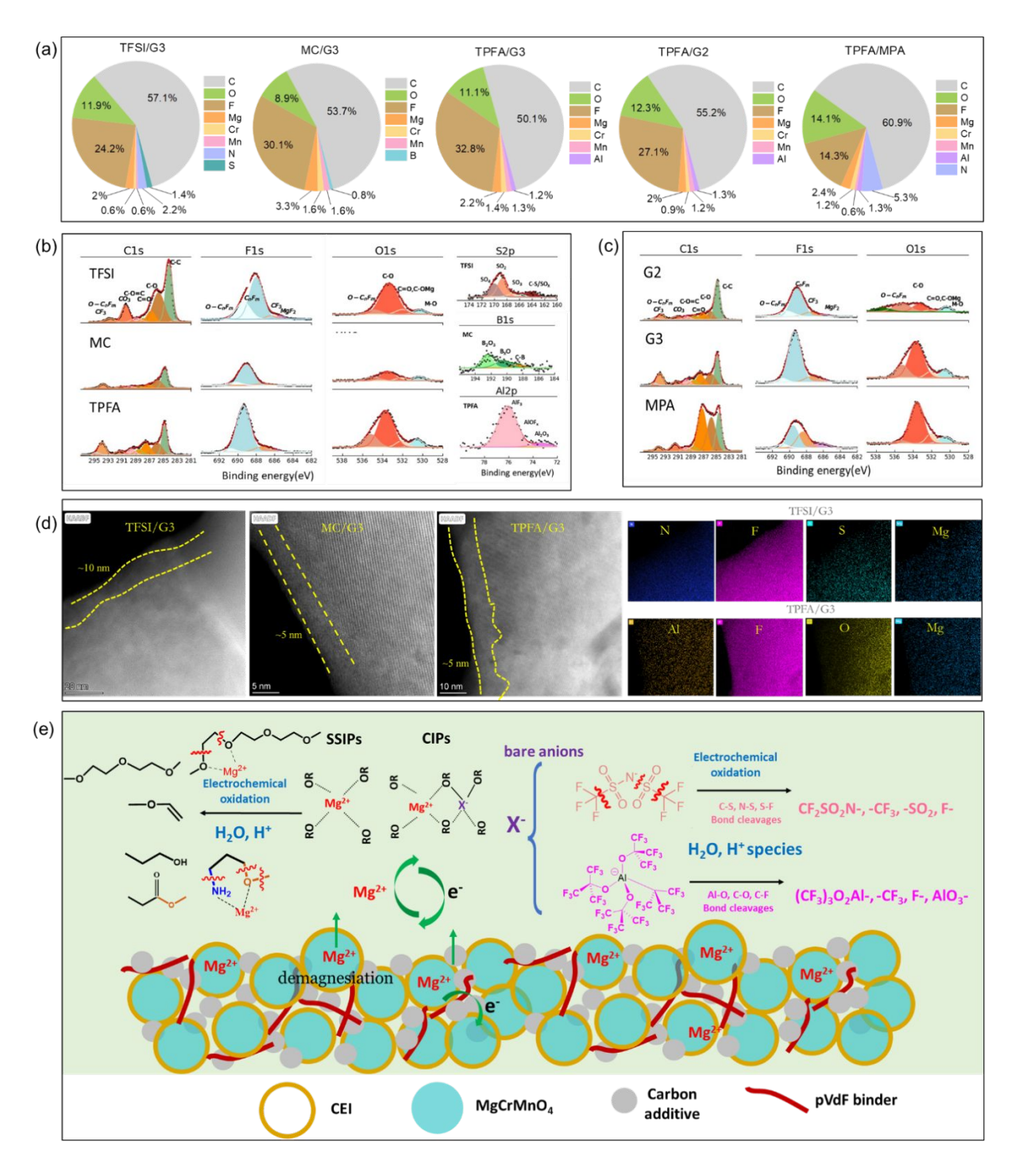


Figure 5. (a) Atomic concentration of surface composition quantified by XPS in TFSI/G3, MC/G3, TPFA/G3, TFPA/G2 and TPFA/MPA. (b) Comparison of high-resolution spectra of three major components in C1s, F1s, and O1s among anion group. The decomposition of anions is represented by S2p (TFSI), B1s (MC) and Al2p (TPFA). Note that F is also observed from MC/G3cell, which is from interaction with pVdF binder. (c) Comparison of high-resolution spectra of three major

components in C1s, F1s, and O1s among solvent group. (d) Representative TEM images and corresponding EDS elemental mappings for CEI thickness and composition. (e) Schematic illustrations of the possible decomposition behavior of anions and solvents at the charged cathode/electrolyte interface

.

2.5 Additive strategy to improve the oxidation stability

The use of electrolyte additives leveraged from LIB has proven to be an effective strategy for fine-tuning the reactivity, electrochemical stability, and surface composition in RMBs.^[27] However, most effort has focused on additives to enhance the stability of the Mg anode, [13, 25, 27] while the investigation of high-voltage additives for the cathode are very limited. To the best of our knowledge, the only reported example involved the utilization of hydrofluoroether solvents (HFEs) with glyme as a co-solvent. [24] HFEs such as 1,1,2,2-tetrafluoroethyl-2,2,3,3tetrafluoropropylether (TTE) was confirmed to improve the oxidative stability while not affecting glyme coordination strength with Mg²⁺ due to its electron withdrawal ability by the electronegative fluorine atoms. [24] Herein, 10 wt.% TTE added in G3 is explored as the candidate electrolyte composition. Mg[TFSI]₂ was selected as demonstration salt for this proof-of-concept due to its commercial availability and ease of synthesis. As shown in Figure 6, the TTE additive lowers the residual current by 16% compared to its baseline. It is also evident that C content decreases significantly, while F, N and S increase in the CEI by XPS analysis (Figure 6b). The primary Fcontaining species are MgF₂ with TTE in the inner layer of CEI, while in baseline, the F-species remain organofluorides (Figure 6c). In addition, Figure 6c shows an increase in the abundance of Mg_xN and Mg-N-C. It appears TTE facilitates greater TFSI⁻ coordination in the solutions, confirmed in FTIR spectra in Figure 6d. The peaks around 1300 cm⁻¹ and 1780 cm⁻¹ intensifies, indicating a commensurate increase in CIP formation with TTE. Clearly, adding TTE to the electrolyte can either act as an F source to increase the amount of MgF₂ in the CEI, or lead to anion-derived inorganic rich CEI composed of Mg_xN. Thus, it can effectively suppress the decomposition of G3 solvent and reduce the leakage current by better passivating MgCrMnO₄ surface prior to reaching potential of 1.2V. The results agree well with the DFT calculations that MgF₂ can be an effective passivating layer to protect high-voltage Mg cathode.^[47] Nonetheless, no substantial enhancement in cycling performance was observed during the initial tests in half cells,

implying other issues including bulk transport properties might offset the beneficial effect of TTE at the interface. The results suggest further engineering optimization such as amount control might be needed to maximize its beneficial effect, given the additive effectiveness often depends on the concentration.

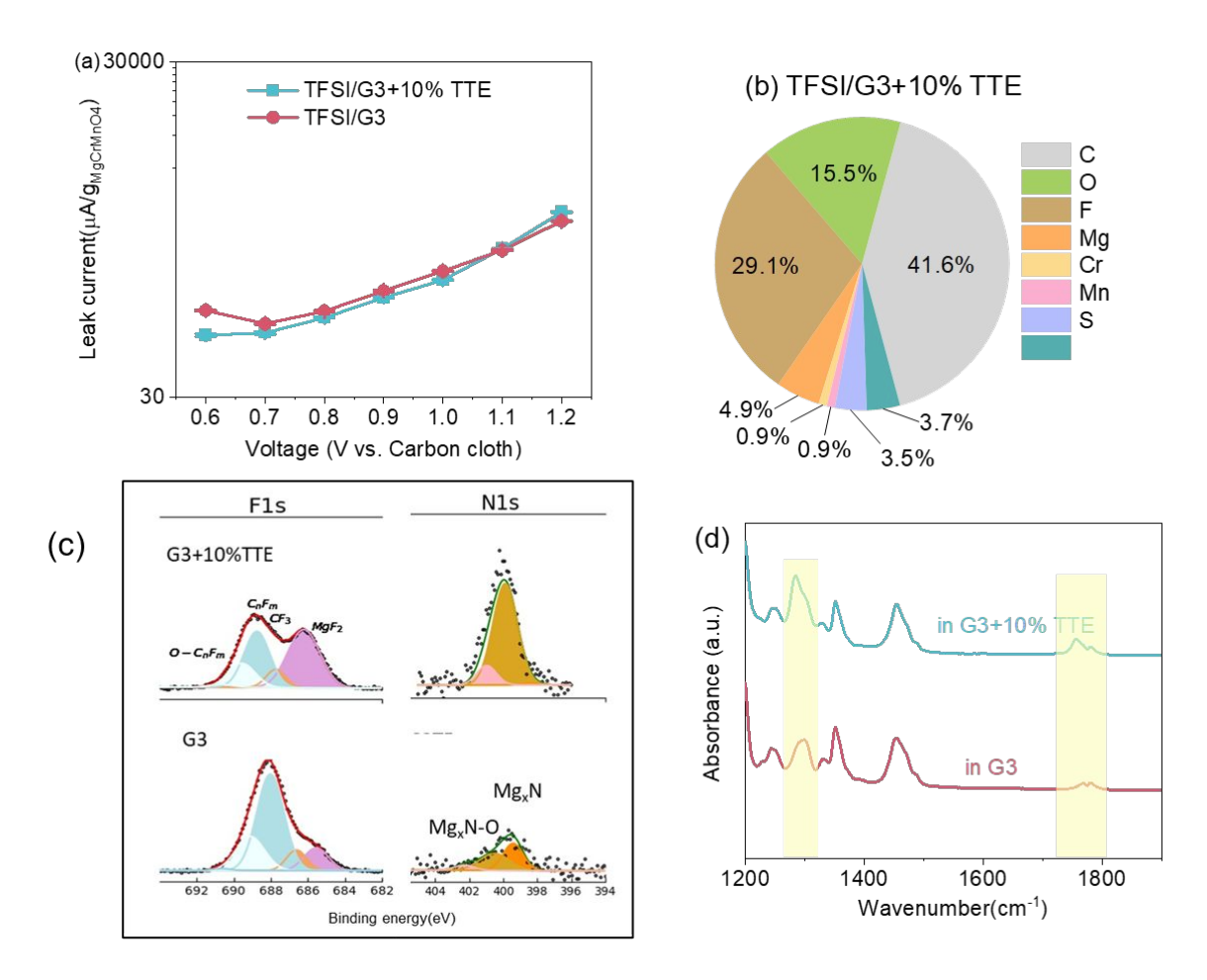


Figure 6. (a) Comparison of the steady state leakage current with/without adding 10wt% TTE in TFSI/G3. (b) Atomic concentration of surface composition quantified by XPS with 10wt% TTE. (c) Comparison of the F1s in the inner layer of CEI after Ar+ ion sputtering. (d) Comparison of FTIR spectra with/without adding 10wt% TTE in TFSI/G3.

3. Conclusions

In this work, we systematically examined the influence of the electrolyte chemistry of anions and solvents on the interfacial reactivity at the interface of MgCrMnO₄ cathode during a potentiostatic hold upon charging. The rate of parasitic reactions was found to be more dependent

on solvent chemistry rather than anion's. TPFA anion with CF₃ electro-withdrawing functional groups can form weak contact ion pairs, yielding improved oxidative stability at the cathode interface by anion derived CEI rich in F compounds. Although amine solvents like 3-methoxypropylamine exhibit strong affinity for Mg²⁺, enhancing Mg plating/stripping performance, they result in higher leakage current and poorer passivation with greater solvent decomposition on cathode compared to glyme-based electrolytes. Future directions will be focused on identifying the combined effect of strong/weak solvent and anion complex formation studied here with improved stability and reversibility on both electrodes. We hope the fundamental understanding in this study can aid in the rational design of innovative electrolyte chemistries and material coatings, ultimately stabilizing the cathode-electrolyte interface toward enabling RMBs with high-voltage Mg metal oxide cathodes.

4. Experimental

Material synthesis. Cathode MgCrMnO₄ was synthesized using an aqueous sol-gel reaction protocol reported by Kwon et al.^[5] The precursors used in the synthesis included magnesium acetate tetrahydrate (Mg(CH₃COO)₂·4H₂O, Sigma-Aldrich), chromium acetate hydroxide (Cr₃(CH₃CO₂)₇(OH)₂, Sigma-Aldrich), and manganese acetate dihydrate (Mn(CH₃COO)₃·4H₂O, Sigma-Aldrich). Citric acid (C₆H₈O₇, Sigma-Aldrich) was employed as a capping agent. For each synthesis, 12.5 mmol of precursors and 25.0 mmol of citric acid were dissolved in 200 mL of deionized water, followed by vigorous stirring for 30 minutes. The resulting mixture was heated to 120 °C to evaporate water until a powder was obtained. The synthesized powders were then calcined in air at 700 °C or 950 °C. The post-MgCrMnO₄ material was obtained by subjecting the initial oxides to post-annealing at 350 °C in air for 24 hours. Mg[TFSI]₂ salt (99.5%) was purchased from Solvionic. Mg[TPFA]₂ salt was synthesized using a method outlined in literature. [23] Mg[CB₁₁H₁₂]₂ salt was synthesized using a previous reported method. [43] Diglyme, triglyme, and 3-methoxypropylamine were obtained from Sigma-Aldrich, purified by vacuum distillation using a 25 cm Vigreux column over CaH₂ and then stored over activated 4A molecular sieves (Sigma-Aldrich) before use. The 0.1M electrolytes, containing various mixtures, were stirred at room temperature for one day to achieve uniform solutions.

Electrode preparation and cell assembly. Cathode laminates were fabricated on stainless-steel (SS) foils, by well mixing 60 wt.% cathode powder with 2 wt.% carbon black conductive agent and 2 wt.% polyvinylidene fluoride (PVDF) binder in 1-methyl-2-pyrrolidone (NMP) solvent. After casting, the cathode laminates underwent drying at 75°C in an air environment overnight, The targeted cathode's mass loading was about 4.0 mg cm⁻². High surface area activated carbon cloth was used as the counter electrode. All laminates were punched into discs with a diameter of 3/8 inch for cathodes and ½ inch for anodes. The punched cathodes and anodes underwent vacuum drying at 80°C for overnight before the assembly of cells. Half cells were assembled using CR2032 coin cell components. Dried Glass microfiber filters at 120°C were used as separators in the coin cells. 100μl of 0.1 M electrolyte was added to each cell.

Electrochemical testing. Electrochemical assessments were conducted using a MACCOR battery cycler at temperatures of 25°C. The reported potentials are referenced with respect to the activated carbon between 0.6V to 1.2V. The nominal C/50 rate was used as the current density based on the theoretical capacity of MgCrMnO₄ (i.e. \sim 280 mAh/g). A custom-designed high-precision leakage current (HpLC) system, constructed using Keithley 2401 source meters, was employed to record the constant leakage current while varying the charging potential. The measurement was held for 30 hr for each potential and 0.1V incremental step was used during charging process until 1.2V. The constant leakage current at each potential was determined by fitting the declining current profile using an exponential decay function (y = A * exp(-x/t) + y0).

Material characterization. The electrolyte structure was probed by reflection-infrared (FTIR) with an FT-IR spectrometer (PerkinElmer, FT/IR-3500) featuring a KBr beam splitter and a single-reflection ATR cell in the glovebox. An optical resolution of 1.0 cm–1 was used, and the spectral data were collected through 64 accumulations for each sample. The surface component of charged cathodes after HpLC test was analyzed by X-ray photoelectron spectroscopy (XPS, PHI 5000 VersaProbe II system) which is attached to an argon-atmosphere glovebox. The spectra were acquired using an Al K-α source (1486.6 eV) with a V-shaped sample focus, an Ar+-ion and electron beam for sample neutralization, fixed analyzer transmission mode, and a pass energy of 46.50 eV. The obtained spectra were calibrated using the C–C peak at 284.8 eV in the C 1s spectrum. TEM imaging and EDX mapping of the cathode materials were conducted using a

Journal of Materials Chemistry A

Page 21 of 25

Thermo Fisher Spectra 200 microscope equipped with a cold field emission gun, operating at 200

kV.

Author contributions

Yang, Z.: conceptualization (lead), investigation (lead), methodology, formal analysis, and writing

of the manuscript; Cai, J.: investigation, formal analysis, and draft editing; Wang, E.: investigation;

Sultanov, M.: investigation; Gao, L.: investigation and resources; Wu, X.: investigation; Liao, C.:

resources, review and editing; Chen, Z.: resources, review and editing; Wen, J., resources; Trahey,

L.: supervision and funding acquisition; Ingram. B.: supervision, review and editing, funding

acquisition and project administration. All authors have given approval to the final version of the

manuscript.

Conflicts of interest

There are no conflicts of interest to declare.

Acknowledgements

This work was led and supported by the Joint Center for Energy Storage Research (JCESR), an

Energy Innovation Hub funded by the U.S. Department of Energy. This research used resources

of the Argonne National laboratory, supported by the U.S. Department of Energy under contract

no. DE-AC02-06CH11357. TEM performed at the Center for Nanoscale Materials, a U.S.

Department of Energy Office of Science User Facility, was supported by the U.S. DOE, Office of

Basic Energy Sciences, under Contract No. DE-AC02-06CH11357.

ORCID

Zhenzhen Yang: 0000-0002-1073-3799

Jiyu Cai: 0000-0003-2283-2281

Evelyna Wang: 0000-0002-5697-474X

Maksim Sultanov: 0000-0002-1191-214X

Chen Liao: 0000-0001-5168-6493

Brian J Ingram: 0000-0002-5219-7517

21

Lynn Trahey: 0009-0000-3580-2466

References

- 1. Johnson, I. D.; Ingram, B. J.; Cabana, J. The Quest for Functional Oxide Cathodes for Magnesium Batteries: A Critical Perspective. *ACS Energy Lett.* **2021**, *6* (5), 1892-1900.
- 2. Aurbach, D.; Suresh, G. S.; Levi, E.; Mitelman, A.; Mizrahi, O.; Chusid, O.; Brunelli, M. Progress in Rechargeable Magnesium Battery Technology. *Adv. Mater.* **2007**, *19* (23), 4260-4267.
- 3. Trahey, L.; Brushett, F. R.; Balsara, N. P.; Ceder, G.; Cheng, L.; Chiang, Y.-M.; Hahn, N. T.; Ingram, B. J.; Minteer, S. D.; Moore, J. S.; Mueller, K. T.; Nazar, L. F.; Persson, K. A.; Siegel, D. J.; Xu, K.; Zavadil, K. R.; Srinivasan, V.; Crabtree, G. W. Energy Storage Emerging: A Perspective from the Joint Center for Energy Storage Research. *Proc. Natl. Acad. Sci. U.S.A.* **2020**, *117* (23), 12550-12557.
- 4. Kwon, B. J.; Lau, K.-C.; Park, H.; Wu, Y. A.; Hawthorne, K. L.; Li, H.; Kim, S.; Bolotin, I. L.; Fister, T. T.; Zapol, P.; Klie, R. F.; Cabana, J.; Liao, C.; Lapidus, S. H.; Key, B.; Vaughey, J. T. Probing Electrochemical Mg-Ion Activity in Mgcr2–Xvxo4 Spinel Oxides. *Chem. Mater.* **2020**, *32* (3), 1162-1171.
- 5. Kwon, B. J.; Yin, L.; Park, H.; Parajuli, P.; Kumar, K.; Kim, S.; Yang, M.; Murphy, M.; Zapol, P.; Liao, C.; Fister, T. T.; Klie, R. F.; Cabana, J.; Vaughey, J. T.; Lapidus, S. H.; Key, B. High Voltage Mg-Ion Battery Cathode Via a Solid Solution Cr–Mn Spinel Oxide. *Chem. Mater.* **2020**, *32* (15), 6577-6587.
- 6. Kwon, B. J.; Yin, L.; Roy, I.; Leon, N. J.; Kumar, K.; Kim, J. J.; Han, J.; Gim, J.; Liao, C.; Lapidus, S. H.; Cabana, J.; Key, B. Facile Electrochemical Mg-Ion Transport in a Defect-Free Spinel Oxide. *Chem. Mater.* **2022**, *34* (8), 3789-3797.
- 7. Liu, M.; Rong, Z.; Malik, R.; Canepa, P.; Jain, A.; Ceder, G.; Persson, K. A. Spinel Compounds as Multivalent Battery Cathodes: A Systematic Evaluation Based on Ab Initio Calculations. *Energy Environ. Sci.* **2015**, *8* (3), 964-974.
- 8. Li, Z.; Häcker, J.; Fichtner, M.; Zhao-Karger, Z. Cathode Materials and Chemistries for Magnesium Batteries: Challenges and Opportunities. *Adv. Energy Mater.* **2023**, *13* (27), 2300682.
- 9. Wang, H.; Ryu, J.; Shao, Y.; Murugesan, V.; Persson, K.; Zavadil, K.; Mueller, K. T.; Liu, J. Advancing Electrolyte Solution Chemistry and Interfacial Electrochemistry of Divalent Metal Batteries. *ChemElectroChem* **2021**, *8* (16), 3013-3029.
- 10. Mohtadi, R.; Tutusaus, O.; Arthur, T. S.; Zhao-Karger, Z.; Fichtner, M. The Metamorphosis of Rechargeable Magnesium Batteries. *Joule* **2021,** *5* (3), 581-617.
- 11. Deivanayagam, R.; Ingram, B. J.; Shahbazian-Yassar, R. Progress in Development of Electrolytes for Magnesium Batteries. *Energy Storage Mater.* **2019**, *21*, 136-153.
- 12. Wang, F.; Hua, H.; Wu, D.; Li, J.; Xu, Y.; Nie, X.; Zhuang, Y.; Zeng, J.; Zhao, J. Solvent Molecule Design Enables Excellent Charge Transfer Kinetics for a Magnesium Metal Anode. *ACS Energy Lett.* **2023**, *8* (1), 780-789.
- 13. Hou, S.; Ji, X.; Gaskell, K.; Wang, P.-f.; Wang, L.; Xu, J.; Sun, R.; Borodin, O.; Wang, C. Solvation Sheath Reorganization Enables Divalent Metal Batteries with Fast Interfacial Charge Transfer Kinetics. *Science* **2021**, *374* (6564), 172-178.
- 14. Zhao, W.; Pan, Z.; Zhang, Y.; Liu, Y.; Dou, H.; Shi, Y.; Zuo, Z.; Zhang, B.; Chen, J.; Zhao, X.; Yang, X. Tailoring Coordination in Conventional Ether-Based Electrolytes for Reversible Magnesium-Metal Anodes. *Angew. Chem. Int. Ed.* **2022**, *61* (30), e202205187.
- 15. Li, C.; Guha, R. D.; Shyamsunder, A.; Persson, K. A.; Nazar, L. F. A Weakly Ion Pairing Electrolyte Designed for High Voltage Magnesium Batteries. *Energy Environ. Sci.* **2024,** *17* (1), 190-201.

- 16. Leon, N. J.; He, M.; Liao, C. Solvation, Rational Design, and Interfaces: Development of Divalent Electrolytes. *Front. Energy Res.* **2022**, *9*, 802398.
- 17. Mohtadi, R.; Matsui, M.; Arthur, T. S.; Hwang, S.-J. Magnesium Borohydride: From Hydrogen Storage to Magnesium Battery. *Angew. Chem. Int. Ed.* **2012,** *51* (39), 9780-9783.
- 18. Luo, J.; Bi, Y.; Zhang, L.; Zhang, X.; Liu, T. L. A Stable, Non-Corrosive Perfluorinated Pinacolatoborate Mg Electrolyte for Rechargeable Mg Batteries. *Angew. Chem. Int. Ed.* **2019**, *58* (21), 6967-6971.
- 19. Tutusaus, O.; Mohtadi, R.; Arthur, T. S.; Mizuno, F.; Nelson, E. G.; Sevryugina, Y. V. An Efficient Halogen-Free Electrolyte for Use in Rechargeable Magnesium Batteries. *Angew. Chem. Int. Ed.* **2015**, *54* (27), 7900-7904.
- 20. Ren, W.; Wu, D.; NuLi, Y.; Zhang, D.; Yang, Y.; Wang, Y.; Yang, J.; Wang, J. An Efficient Bulky Mg[B(Otfe)4]2 Electrolyte and Its Derivatively General Design Strategy for Rechargeable Magnesium Batteries. *ACS Energy Lett.* **2021**, *6* (9), 3212-3220.
- 21. Herb, J. T.; Nist-Lund, C. A.; Arnold, C. B. A Fluorinated Alkoxyaluminate Electrolyte for Magnesium-Ion Batteries. *ACS Energy Lett.* **2016**, *1* (6), 1227-1232.
- 22. Tang, K.; Du, A.; Du, X.; Dong, S.; Lu, C.; Cui, Z.; Li, L.; Ding, G.; Chen, F.; Zhou, X.; Cui, G. A Novel Regulation Strategy of Solid Electrolyte Interphase Based on Anion-Solvent Coordination for Magnesium Metal Anode. *Small* **2020**, *16* (49), 2005424.
- 23. Lau, K.-C.; Seguin, T. J.; Carino, E. V.; Hahn, N. T.; Connell, J. G.; Ingram, B. J.; Persson, K. A.; Zavadil, K. R.; Liao, C. Widening Electrochemical Window of Mg Salt by Weakly Coordinating Perfluoroalkoxyaluminate Anion for Mg Battery Electrolyte. *J. Electrochem. Soc.* **2019**, *166* (8), A1510-A1519.
- 24. Hahn, N. T.; Kamphaus, E. P.; Chen, Y.; Murugesan, V.; Mueller, K. T.; Cheng, L.; Zavadil, K. R. Magnesium Battery Electrolytes with Improved Oxidative Stability Enabled by Selective Solvation in Fluorinated Solvents. *ACS Appl. Energy Mater.* **2023**, *6* (6), 3264-3277.
- Zhang, D.; Wang, Y.; Yang, Y.; Zhang, Y.; Zhao, Y.; Pan, M.; Sun, Y.; Chen, S.; Liu, X.; Wang, J.; NuLi, Y. Constructing Efficient Mg(Cf3so3)2 Electrolyte Via Tailoring Solvation and Interface Chemistry for High-Performance Rechargeable Magnesium Batteries. *Adv. Energy Mater.* **2023**, *13* (39), 2301795.
- 26. Drews, J.; Jankowski, P.; Häcker, J.; Li, Z.; Danner, T.; García Lastra, J. M.; Vegge, T.; Wagner, N.; Friedrich, K. A.; Zhao-Karger, Z.; Fichtner, M.; Latz, A. Modeling of Electron-Transfer Kinetics in Magnesium Electrolytes: Influence of the Solvent on the Battery Performance. *ChemSusChem* **2021**, *14* (21), 4820-4835.
- 27. Forero-Saboya, J. D.; Tchitchekova, D. S.; Johansson, P.; Palacín, M. R.; Ponrouch, A. Interfaces and Interphases in Ca and Mg Batteries. *Adv. Mater. Interfaces* **2022**, *n/a* (n/a), 2101578.
- 28. Sa, N.; Mukherjee, A.; Han, B.; Ren, Y.; Klie, R. F.; Key, B.; Vaughey, J. T. Direct Observation of Mgo Formation at Cathode Electrolyte Interface of a Spinel Mgco2o4 Cathode Upon Electrochemical Mg Removal and Insertion. *J. Power Sources* **2019**, *424*, 68-75.
- 29. Seguin, T. J.; Hahn, N. T.; Zavadil, K. R.; Persson, K. A. Elucidating Non-Aqueous Solvent Stability and Associated Decomposition Mechanisms for Mg Energy Storage Applications from First-Principles. *Front. Chem.* **2019**, *7*, 175.
- 30. Fujii, K.; Sogawa, M.; Yoshimoto, N.; Morita, M. Structural Study on Magnesium Ion Solvation in Diglyme-Based Electrolytes: Ir Spectroscopy and Dft Calculations. *J. Phys. Chem. B* **2018**, *122* (37), 8712-8717.
- 31. Kimura, T.; Fujii, K.; Sato, Y.; Morita, M.; Yoshimoto, N. Solvation of Magnesium Ion in Triglyme-Based Electrolyte Solutions. *J. Phys. Chem. C* **2015**, *119* (33), 18911-18917.
- 32. Hua, H.; Wang, F.; Wang, F.; Wu, J.; Xu, Y.; Zhuang, Y.; Zeng, J.; Zhao, J. Machine Learning Molecular Dynamics Insight into High Interface Stability and Fast Kinetics of Low-Cost Magnesium

Chloride Amine Electrolyte for Rechargeable Magnesium Batteries. *Energy Storage Mater.* **2024,** *70,* 103470.

- 33. Rajput, N. N.; Seguin, T. J.; Wood, B. M.; Qu, X.; Persson, K. A. Elucidating Solvation Structures for Rational Design of Multivalent Electrolytes—a Review. *Top. Curr. Chem.* **2018**, *376* (3), 19.
- 34. Yang, Z.; Gao, L.; Leon, N. J.; Liao, C.; Ingram, B. J.; Trahey, L. Quantifying the Correlation between Coordination Chemistry, Interfacial Formation, and Electrochemical Performances for Mg Battery Electrolytes. *ACS Appl. Energy Mater.* **2024**, *7* (4), 1666-1675.
- 35. Yang, Z.; Yang, M.; Hahn, N. T.; Connell, J.; Bloom, I.; Liao, C.; Ingram, B. J.; Trahey, L. Toward Practical Issues: Identification and Mitigation of the Impurity Effect in Glyme Solvents on the Reversibility of Mg Plating/Stripping in Mg Batteries. *Front. Chem.* **2022**, *10*, 966332.
- 36. Connell, J. G.; Genorio, B.; Lopes, P. P.; Strmcnik, D.; Stamenkovic, V. R.; Markovic, N. M. Tuning the Reversibility of Mg Anodes Via Controlled Surface Passivation by H2o/Cl– in Organic Electrolytes. *Chem. Mater.* **2016**, *28* (22), 8268-8277.
- 37. Tomich, A. W.; Chen, J.; Carta, V.; Guo, J.; Lavallo, V. Electrolyte Engineering with Carboranes for Next-Generation Mg Batteries. *ACS Cent. Sci.* **2024**, *10* (2), 264-271.
- 38. Mruthunjaya, A. K. V.; Torriero, A. A. J. Mechanistic Aspects of the Electrochemical Oxidation of Aliphatic Amines and Aniline Derivatives. *Molecules* **2023**, *28* (2), 471.
- 39. Yin, L.; Kwon, B. J.; Choi, Y.; Bartel, C. J.; Yang, M.; Liao, C.; Key, B.; Ceder, G.; Lapidus, S. H. Operando X-Ray Diffraction Studies of the Mg-Ion Migration Mechanisms in Spinel Cathodes for Rechargeable Mg-Ion Batteries. *J. Am. Chem. Soc.* **2021**, *143* (28), 10649-10658.
- 40. Doyle, M.; Fuller, T. F.; Newman, J. Modeling of Galvanostatic Charge and Discharge of the Lithium/Polymer/Insertion Cell. *J. Electrochem. Soc.* **1993**, *140* (6), 1526.
- 41. Vadivel, N. R.; Ha, S.; He, M.; Dees, D.; Trask, S.; Polzin, B.; Gallagher, K. G. On Leakage Current Measured at High Cell Voltages in Lithium-Ion Batteries. *J. Electrochem. Soc.* **2017**, *164* (2), A508.
- 42. Cai, J.; Yang, Z.; Zhou, X.; Wang, B.; Suzana, A.; Bai, J.; Liao, C.; Liu, Y.; Chen, Y.; Song, S.; Zhang, X.; Wang, L.; He, X.; Meng, X.; Karami, N.; Ali Shaik Sulaiman, B.; Chernova, N. A.; Upreti, S.; Prevel, B.; Wang, F.; Chen, Z. Unveiling the Parasitic-Reaction-Driven Surface Reconstruction in Ni-Rich Cathode and the Electrochemical Role of Li2co3. *J. Energy Chem.* **2023**, *85*, 126-136.
- 43. Hahn, N. T.; Seguin, T. J.; Lau, K.-C.; Liao, C.; Ingram, B. J.; Persson, K. A.; Zavadil, K. R. Enhanced Stability of the Carba-Closo-Dodecaborate Anion for High-Voltage Battery Electrolytes through Rational Design. *J. Am. Chem. Soc.* **2018**, *140* (35), 11076-11084.
- 44. Xie, Y.; Gao, H.; Gim, J.; Ngo, A. T.; Ma, Z.-F.; Chen, Z. Identifying Active Sites for Parasitic Reactions at the Cathode–Electrolyte Interface. *J. Phys. Chem. Lett.* **2019**, *10* (3), 589-594.
- 45. Zhou, W.; Xu, C.; Gao, B.; Nakayama, M.; Yagi, S.; Tateyama, Y. Glyme Solvent Decomposition on Spinel Cathode Surface in Magnesium Battery. *ACS Energy Lett.* **2023**, *8* (10), 4113-4118.
- 46. Xie, X.; Leon, N. J.; Small, D. W.; Spotte-Smith, E. W. C.; Liao, C.; Persson, K. A. Reductive Decomposition Kinetics and Thermodynamics That Govern the Design of Fluorinated Alkoxyaluminate/Borate Salts for Mg-Ion and Ca-Ion Batteries. *J. Phys. Chem. C* **2022**, *126* (49), 20773-20785.
- 47. Chen, T.; Ceder, G.; Sai Gautam, G.; Canepa, P. Evaluation of Mg Compounds as Coating Materials in Mg Batteries. *Frontiers in Chemistry* **2019**, *7*.

Data availability statements

The data that support the findings of this study are available from the corresponding author upon reasonable request.